CHAPTER 1

Elastic Fibers in Flows

ANKE LINDNER[1], MICHAEL SHELLEY[2]

[1]Laboratoire de Physique et Mécanique des Milieux Hétérogenes, UMR7636, CNRS, ESPCI Paristech, Université Pierre et Marie Curie, Université Paris Diderot, 10 rue Vauquelin, 75005 Paris, France.
[2]Applied Math Lab, Courant Institute of Mathematical Sciences, New York University, New York, NY 10012, USA

RSC Soft Matter No. 1
Fluid-structure interactions at low Reynolds numbers
Edited by Camille Duprat and Howard A. Stone

Published by the Royal Society of Chemistry, www.rsc.org

1.1 Introduction

A very common class of fluid-structure interaction problems involves the dynamics of flexible fibers immersed in a Stokesian fluid. In biology this arises in modeling the flagellae or cilia involved in micro-organismal locomotion and mucal transport, in determining the shape of biofilm streamers, and in understanding how biopolymers such as microtubules respond to the active coupling afforded by motor proteins. In engineering it arises in the paper processing industry, where wood pulp suspensions can show the abrupt appearance of normal stress differences, and in micro-fluidic engineering where flow control using flexible particles has lately been explored. Flow induced buckling of fibers is an important determinant on fiber transport in those flows, as well as for the fluid mechanical stresses that develop.

Over the past decade, the dynamics of immersed fibers has been studied intensively, particularly through theoretical means. Specialized numerical methods, such as those based on slender body theory or other methods, have been developed to efficiently simulate their dynamics in a variety of flow situations. On the experimental side, recent advances in micro-fabrication and flow control have led to an increasing number of experimental studies. Both theoretical and experimental studies have identified and studied canonical buckling instabilities of fibers under flow forcing, though experimental work is still lacking in precisely linking fiber deformation to fiber transport. A practical understanding could be used in a variety of applications. For example, by linking deformation and transport to applied flow rate in specific flow geometries, new flow sensors or separation devices could be designed. On both the theoretical and experimental side, there is, as yet, little understood of how the macroscopic properties of fiber suspensions depend upon the microscopic dynamics of flexible fibers. Such an understanding would yield better control and exploitation of such systems.

1.2 Mathematical Modeling

The interaction of elastic fibers with flows is a specialized type of fluid structure interaction for which specialized mathematical descriptions and computational methods have been developed. The most basic and easy to use of these is local slender-body theory (SBT), which gives a local anisotropic relation between elastic and drag forces. Nonlocal hydrodynamic interactions can be captured through use of higher order, more complex, slender-body formulations, or through other approaches such as immersed boundary methods, bead-rod models, or regularized Stokeslet methods.

1.2.1 Background

To set the stage, consider a slender elastic fiber of length L, of circular cross-section with radius a (hence $\epsilon = a/L << 1$), and flexural rigidity $E = YI$ with Y the material Youngs modulus and I the areal moment of inertia ($I = \pi a^4/4$). This fiber is immersed in a Newtonian fluid of shear viscosity μ with the fluid motion characterized by a strain-rate $\dot{\gamma}$. Neglecting inertial forces in both fluid and fiber, three important forces are in play: Brownian forces $\sim kT/L$, drag forces $\sim \mu\dot{\gamma}L^2$, and elasticity forces $\sim Ya^4/L^2$. For most of the work reviewed here, though not all, drag and elasticity forces dominate Brownian forces. That predominance requires that

$L >> L_1 = (kT/\mu\dot{\gamma})^{1/3}$ and $L >> L_2 = (kT/Y\epsilon^4)^{1/3}$. Taking water as the solvent, a fluid strain-rate of $\dot{\gamma} = 1\ s^{-1}$, a fiber of aspect ratio $\epsilon = 10^{-3}$, and a material modulus of $Y = 1\ GPa$, we find $L_1 = L_2 = 1\ \mu m$.

1.2.2 A Simple Beam Model

Again, consider a slender elastic filament of length L, a circular cross-section of radius a at its midpoint, and centerline position $\mathbf{X}(s,t)$ with $-L/2 \leq s \leq L/2$ its signed arclength. The immersing fluid is assumed to be Newtonian with viscosity μ, and the flow is assumed to be "slow" so that $Re << 1$ and the fluid dynamics is described by the Stokes equations. The suspending Stokesian fluid exerts surface stresses upon the fiber, which are balanced by its bending and tensile forces. Perhaps the simplest nonlinear model of these elastic forces is given by the inextensible Euler-Bernoulli beam, for which

$$\mathbf{f}(s,t) = -E\mathbf{X}_{ssss} + (T(s,t)\mathbf{X}_s)_s \tag{1.1}$$

Here $\mathbf{f}$ has units of force per unit length and can be considered as the surface stress circumferentially averaged around the fiber. The first term is the bending force (per unit length) with E the flexural rigidity. Subscripts refer to partial differentiation. The second term is the tensile force (per unit length) with T being the "axial tension". The role of the tension is to enforce the condition of inextensibility that states that the arclength s gives a material parametrization of the filament centerline and so s and t are independent variables. Hence, $\partial_{st} = \partial_{ts}$, which generates a constraint on the centerline velocity $\mathbf{X}_t = \mathbf{V}$ as follows: That s is arclength means that $\mathbf{X}_s \cdot \mathbf{X}_s = 1$, and so $0 = \partial_t \mathbf{X}_s \cdot \mathbf{X}_s = 2\mathbf{X}_s \cdot \mathbf{X}_{st} = 2\mathbf{X}_s \cdot \mathbf{X}_{ts} = 2\mathbf{X}_s \cdot \mathbf{V}_s$. That is, $\mathbf{X}_s \cdot \mathbf{V}_s = 0$, which is a scalar constraint that is satisfied through determination of the scalar tension T. Note that in a Stokesian fluid, velocities depend linearly upon forces, and so this constraint is a linear equation for T.

1.2.3 Local SBT

One approach to modeling the dynamics of an immersed flexible fiber is based on slender body theory, which exploits the large aspect ratio of the fibers by using the slenderness ratio $\epsilon = a/L$ as an expansion variable. The simplest and most popular version is the leading-order local drag model [1] which gives a local relation between the velocity of the filament centerline and the force per unit length, $\mathbf{f}$, that the filament exerts on the fluid:

$$8\pi\mu\left(\mathbf{V}(s,t) - \mathbf{u}(\mathbf{X}(s,t),t)\right) = c\mathbf{D}\mathbf{f}(s,t) \tag{1.2}$$

Here $\mathbf{u}(\mathbf{x},t)$ is a given background flow, $c = -\ln(\epsilon^2 e)$, reflecting that SBT is logarithmic at leading-order, and the tensor $\mathbf{D} = \mathbf{I} + \mathbf{X}_s\mathbf{X}_s^T$ arises from drag anisotropy.

For an elastic fiber modeled as an inextensible Euler-Bernoulli beam, the viscous force balances the elastic force and we have the equations

$$\mathbf{V} = \mathbf{u}(\mathbf{X},t) + \frac{c}{8\pi\mu}\mathbf{D}\left(-E\mathbf{X}_{ssss} + (T\mathbf{X}_s)_s\right) \tag{1.3}$$

$$\mathbf{X}_s \cdot \mathbf{V}_s = 0 \tag{1.4}$$

Applying the constraint (1.4) to Eq. (1.3) for $\mathbf{V}$ yields an elliptic equation for T of the form:

$$2T_{ss} - |\mathbf{X}_{ss}|^2 T = R(s) \tag{1.5}$$

The righthand side R in Eq. (1.5) is determined by the background flow and the bending force. Given appropriate boundary conditions, such as $T = 0$ for a "force-free" fiber, Eq. (1.5) has a unique solution T, and Eq. (1.3) can be used to evolve the fiber's shape, position, and orientation. Assume that the background flow has a characteristic length-scale W and time-scale $\dot{\gamma}^{-1}$ and can be expressed as $\mathbf{u} = \dot{\gamma} W \mathbf{U}(\mathbf{x}/W, \dot{\gamma} t)$ in terms of a dimensionless background velocity $\mathbf{U}$. Then by scaling space on L, time on $\dot{\gamma}^{-1}$, and T on E/L^2, we can rewrite the dynamics equation (i.e. $\mathbf{X}_t = \mathbf{V}$) in the adimensional form:

$$\mathbf{V} = \alpha^{-1} \mathbf{U}(\alpha \mathbf{X}, t) - \eta^{-1} \mathbf{D} \left(\mathbf{X}_{ssss} - (T \mathbf{X}_s)_s \right) \tag{1.6}$$

where $\alpha = L/W$, and $\eta = 8\pi\mu\dot{\gamma}L^4/Ec$ is the effective strength of flow forcing. Note that if the tension is negative, and so fluid stresses are compressive, then in Eq. (1.6) is seen the competition of a fourth-order diffusion and a second-order anti-diffusion. Note further that if $\mathbf{U}$ is a linear flow then the parameter α cancels out from the dynamics.

1.2.4 Nonlocal SBT and other methods

Nonlocal SBT

The primary appeal of using local SBT lies in its reduction of filament/fluid interaction to a relatively simple dynamics equation for the filament centerline. However, local SBT neglects non-local hydrodynamic interactions, and while such interactions are actually of higher order in ϵ, they are only weakly separated from the leading order term by a factor logarithmic in ϵ (i.e. the next-order terms in Eq. (1.2) are $O(1)$). Local drag models do not include interactions mediated by the intervening incompressible fluid, be they from the filament itself or from other filaments and structures in the fluid.

Different methods have been developed that account for such nonlocal interactions. Keller and Rubinow [1] developed a non-local SBT that captures the global effect on the fluid velocity arising from the presence of the filament, making use of the theory of fundamental solutions for Stokes flow [2]. Their approach yields an integral equation with a modified Stokeslet kernel on the filament centerline that relates the filament forces to the velocity of the centerline. Johnson [3] added a more detailed analysis and a modified formulation that included accurate treatment of the filament's free ends, yielding an equation that is asymptotically accurate to $O(\epsilon^2 \log \epsilon)$. Götz [4] also derived a nonlocal SBT, and performed a detailed analysis of the case of straight filaments, establishing a connection with Legendre polynomials. Shelley & Ueda [5, 6] were the first to design a numerical method based on a non-local SBT for simulating flexible filaments. Their interest was in understanding the dynamics of a growing and buckling flexible filament, motivated by observations of phase transitions in smectic-A liquid crystals.

Tornberg & Shelley [7] developed a stable and numerically tractable version of nonlocal SBT for flexible filaments with free-ends, and for this formulation devised specialized quadrature schemes for nearly singular integrals and efficient implicit time-stepping methods that removed the time-step constrained associated with the bending forces. In their formulation,

Eq. (1.2) is replaced by

$$8\pi\mu(\mathbf{V}-\mathbf{U}) = -\mathbf{\Lambda}[\mathbf{f}] - \mathbf{K}_\delta[\mathbf{f}] \tag{1.7}$$

where

$$\mathbf{\Lambda}[\mathbf{f}] = \left[(c+1)\mathbf{I} + (c-3)\mathbf{X}_s\mathbf{X}_s^T\right]\mathbf{f} \tag{1.8}$$

is a local operator whose leading order logarithmic behavior is given by $c\mathbf{D}$, and

$$\mathbf{K}_\delta = \int_0^1 ds' \left(\frac{\mathbf{I}+\hat{\mathbf{R}}(s,s')\hat{\mathbf{R}}(s,s')^T}{(|\mathbf{R}(s,s')|^2+\delta^2(s))^{1/2}}\mathbf{f}(s') - \frac{\mathbf{I}+\mathbf{X}_s\mathbf{X}_s^T}{(|s-s'|^2+\delta^2(s))^{1/2}}\mathbf{f}(s) \right) \tag{1.9}$$

is an $O(\epsilon^0)$ nonlocal operator that captures filament self-interaction, and $\hat{\mathbf{R}} = \mathbf{R}/|\mathbf{R}|$ with $\mathbf{R}(s,s') = \mathbf{X}(s) - \mathbf{X}(s')$. Here $\delta(s) \sim O(\epsilon)$ is a function whose inclusion cuts off the growth of high-wavelength modes that are treated inaccurately by slender-body theory (see Tornberg & Shelley [7] for a detailed explanation and analysis). Götz' [4] analysis also gave integral expressions, in terms of Stokeslet and dipole distributions, for the induced fluid velocity around the filament, and Tornberg & Shelley used these results to simulate the dynamics of suspensions of interacting flexible filaments moving in a background shear flow.

Tornberg & Gustavsson [8] exploited the connection between Legendre polynomials and nonlocal SBT [4] to develop accurate methods for evolving suspensions of rigid filaments. Saintillan, Shaqfeh, & Darve [9] used low order versions of such representations to evolve large systems of settling fibers.

The Immersed Boundary Method

The immersed boundary method [10] has also been applied to this class of problems. In this method, a filament is discretized with connected Lagrangian markers, and their relative displacements by fluid motions are used to calculate the filament's elastic response. These elastic forces are then distributed onto a background grid covering the fluid volume, and are used as forces acting upon the fluid, thus modifying the fluid flow. The advantage of the immersed boundary method is that detailed immersed mechanical structures can be simulated, but at the cost of having to solve the flow equations in the entire fluid volume. Stockie & Green [11] used an immersed boundary method (at moderate Reynolds number) to simulate a single filament buckling in a linear shear-flow. The filament was treated as an infinitely thin elastic boundary in a two-dimensional flow and discretized using 40 to 80 Lagrangian markers. In this case, the fiber width is artificial and is set by elements of the numerical discretization.

Within this method if the fiber is to have a physical width, a fiber microstructure must be constructed (see, for example, Lim & Peskin [12]). Perhaps the most numerically sophisticated application of the immersed boundary method, relevant to this review, is work by Nguyen & Fauci [13], who study the dynamics of flexible fibers as models, in part, for diatom chains (diatoms are nonmotile unicellular phytoplankton). They employ an adaptive-grid version of the immersed boundary method [14] and investigate fibers that are composite structures made of alternating segments that mimic the structure of diatom chains. While a simple beam model, like Eq. (1.6), describes its bending deformations well, the results of compressive strains are not.

Bead-and-Rod Models

While not always theoretically well-separated from approaches based upon SBT or the immersed boundary method, bead-and-rod models have a somewhat independent lineage from these other methods. In bead-and-rod models, a flexible fiber is represented as a one-dimensional chain of linked rigid bodies (e.g. spheres, spheroids, rods) that experience local drag and interact with each other through short-range forces (e.g. repulsion, lubrication, friction), while sometimes neglecting long-ranged hydrodynamic interactions or only including a subset of them. A recent review of these methods is found in Hämäläinen *et al.* [15]. One example of a merging of modeling and computational methodologies is found in Lindström and Uesaka [16], who develop a hybrid of the method by Switzer and Klingenberg [17], where the fiber is treated as a linked chain of ellipsoids, and an immersed boundary method [10] where fiber forces drive the immersing fluid motions through a coupling term in the large-scale momentum equations. Delmotte *et al.* [18] have elaborated upon basic bead models by introducing a new Lagrange multiplier method to impose constraints, and consider several flow problems – Jeffery orbits, buckling in shear, actuated swimming filaments – using an approximate accounting of the Stokesian hydrodynamics.

The Regularized Stokeslet Method

Another method for approximately solving the Stokes equations is the method of regularized Stokeslets of Cortez [19]. Like a boundary integral method [2], the dynamics is formulated using superpositions of Green's function solutions of the Stokes equations, though in a regularized form. Flores *et al.* [20] use a superposition of regularized Stokeslets and Rotlets to simulate the dynamics of driven flagellae. In their study, a flagellum is a network of flexible springs, and a helical shape so composed is driven by a torque at its base. See Smith [21] for an interesting version of regularized Stokeslets that utilizes a boundary-element approach to the discretization, and incorporates the presence of walls. Bouzarth *et al.* [22] use a regularized representation of a one-dimensional curve of two-dimensional Stokeslets to simulate the nonlocal dynamics of flexible, slightly extensible fibers. Olson *et al.* [23] have recently combined the regularized Stokeslet method for evolving slender rods with the internal mechanics of an elastica with intrinsic twist and curvature.

1.3 Experimental Techniques

Systematic studies of the dynamics of elastic fibers in low Reynolds number flows require a precise control of the flow geometry, as well as the fiber properties. In addition, the determination of fiber position, orientation, and shape as functions of time requires the direct visualization of the fiber under flow.

While several pioneering works have observed fiber dynamics in macroscopic systems [24, 25], these investigations were limited to a small number of flow geometries and did not capture the whole complexity of the fiber dynamics. In recent years the development of micro-fluidics and new micro-fabrication techniques have helped to overcome these difficulties. Micro-fluidic flow devices [26] are now commonly used and allow for the simple and precise control of flow geometry. Due to the small size of these devices, high velocity gradients can be reached

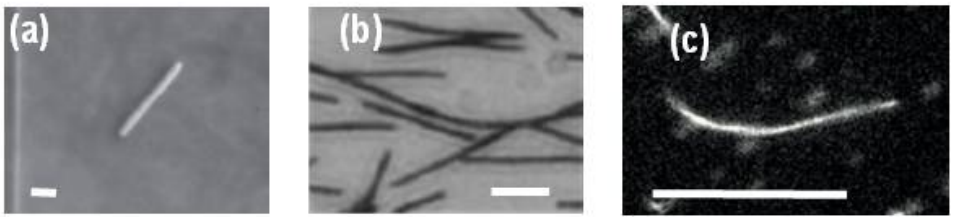

Figure 1.1: Model fibers fabricated by (a) projection lithography, (b) self-assembly of magnetic colloids, and (c) polymerization of actin filaments (courtesy O. du Roure, PMMH-ESPCI). The scale bar represents 10 μm on each image.

while keeping flow inertia small. In combination with recent micro-fabrication techniques they have become a powerful tool for studying fluid-structure interactions between elastic fibers and viscous flows.

The micro-fabrication of fibers often aims at the synthesis of very long filaments (see [27] and references therein) and less attention has been paid to the fabrication of fibers of well-controlled shape and elastic properties. An example of the fabrication of fiber suspensions can be found in a recent study [28, 29] that implemented two different fabrication techniques, one based on a UV projection method developed by Dendukuri *et al* [30, 31], and another using auto-assembly of paramagnetic colloids [32], to fabricate fibers directly inside of micro-fluidic channels (see Fig. 1.1). With the *in-situ* characterization of fiber mechanical properties (i.e., bending modulus) [33, 34], these then yield very well-controlled experimental model systems. Another approach is to make use of elastic bio-polymers such as actin [35–37] or microtubules [38], where in the former case Brownian fluctuations can play a role. Fluorescent labeling techniques make a direct visualization of these bio-polymers under flow possible.

1.4 Simulations and Observations

1.4.1 Instabilities of Fibers

How fibers are buckled by flow is of central importance to much of the interesting nonlinear dynamics observed in simulations and experiments of fiber motion. Here we first discuss a prototypical situation where buckling arises as an instability to an otherwise straight fiber – a straight fiber moving in a linear background flow. We then discuss other prototypical problems such as the buckling of a fiber held fixed against an impinging flow, and the buckling of flexible fibers sedimenting under gravitational load.

The stability of free fibers in linear flows - Mathematical analysis

Because of its relative simplicity, local SBT is usually the preferred formulation for studying linear stability of immersed fibers. Here we first consider fibers moving freely in the flow which means that they are force and torque free particles. This constraint is satisfied by the so-called free-end boundary conditions: $T|_{s=\pm 1/2} = 0$ and $\mathbf{X}_{ss}|_{s=\pm 1/2} = \mathbf{X}_{sss}|_{s=\pm 1/2} = \mathbf{0}$. A perfectly straight isolated fiber will remain straight in any linear background flow, making this a suitable

base-state for linear stability analysis. Hence, we assume that the background flow is linear and incompressible, that is $\mathbf{U}(\mathbf{x}) = \mathbf{A} \cdot \mathbf{x}$ with $tr(\mathbf{A}) = 0$. A straight fiber can be represented as $\mathbf{X}(s,t) = \mathbf{X}_c(t) + s\mathbf{e}(t)$ with $\mathbf{X}_c$ its center point, and $\mathbf{e}$ a unit orientation vector. Inserting this form into Eqs. (1.6) & (1.5), and applying the conditions of zero total force and torque, yields

$$\dot{\mathbf{X}}_c = \mathbf{A}\mathbf{X}_c, \;\; \dot{\mathbf{e}} = \left(\mathbf{I} - \mathbf{e}\mathbf{e}^T\right)\mathbf{A}\mathbf{e}, \;\; \bar{T} = -\frac{\eta}{4}(\mathbf{e}^T\mathbf{E}\mathbf{e})(s^2 - 1/4) \tag{1.10}$$

where $\mathbf{E} = (\mathbf{A} + \mathbf{A}^T)/2$ is the symmetric rate-of-strain tensor. Hence, the rod center is carried with the local flow, the orientation vector obeys Jeffrey's equation [39], and the tension $\bar{T}$ is quadratic in s^2 with its sign determined by the orientation of $\mathbf{e}$ relative to the principle axes of $\mathbf{E}$. Thus, if the fiber is aligned with compressive straining of the flow then the tension is negative and hence compressive. This is the necessary condition for buckling.

The case of 2D flow, with the fiber moving in the 2D plane, is particularly simple. By linearizing Eqs. (1.5) & (1.6) about the straight-fiber solution found in Eqs. (1.10), one can find a scalar equation governing the amplitude w of an in-plane perturbation transverse to the fiber:

$$\eta\left(w_t - (\mathbf{e}_\perp^T\mathbf{A}\mathbf{e}_\perp)w\right) = 2\bar{T}_s w_s + \bar{T}w_{ss} - w_{ssss} \tag{1.11}$$

with boundary conditions $w_{ss}|_{s=\pm 1/2} = w_{sss}|_{s=\pm 1/2} = 0$, and where $\mathbf{e}_\perp = (-e_y, e_x)$. This is a variable coefficient, generally time-dependent equation.

The most straightforward, illustrative case is given by a simple straining flow $\mathbf{u} = (x, -y)$ where the fiber is moving along the y-axis, which is the direction of flow compression [40]. Then $\mathbf{e} = \hat{\mathbf{y}}$ and $\mathbf{e}_\perp = -\hat{\mathbf{x}}$ so that $\mathbf{e}_\perp^T\mathbf{A}\mathbf{e}_\perp = 1$, $\mathbf{e}^T\mathbf{A}\mathbf{e} = -1$, and $\bar{T} = \frac{\eta}{4}(s^2 - 1/4)$ (which is negative). For this case, note the lack of any explicit time-dependence from the background flow. Setting $w = e^{\lambda t}f$ we can consider the time-independent eigenvalue problem

$$\lambda f = f + sf_s + \frac{1}{4}\left(s^2 - 1/4\right)f_{ss} - \eta^{-1}f_{ssss} \tag{1.12}$$

While the variable coefficient nature prevents a closed-form solution, one can easily solve this eigenvalue/eigenfunction problem numerically. For this we discretize (1.12) using second-order finite-differences that are symmetric at interior mesh points, and asymmetric near the boundaries $s = \pm 1/2$. The boundary conditions are represented as asymmetric difference formulae that couple the unknown boundary values of f (at $s = \pm 1/2$) to its unknown interior values. The approach is identical to that used by Tornberg and Shelley for evolving elastic fiber flows using nonlocal SBT [7]; see also [36, 40].

With an eigenvalue solver we can track the system's eigenvalues and eigenfunctions as η, the effective viscosity or strain-rate, is increased. For small η the straight fiber is stable to perturbations. With increase in η we find the successive crossing to the right half-plane of eigenvalues coupled to eigenfunctions associated with increasingly higher order bending modes. The first three crossings occur at $\eta_1 = 153.2$, $\eta_2 = 774.3$, and $\eta_3 = 1930$, and their associated eigenfunctions are shown in Fig. 1.2b. These are classical buckling modes.

An earlier related analysis was performed by Becker and Shelley [41] for the case of a fiber rotating in a linear shear flow. There the focus was on the fiber dynamics as it rotated through the flow quadrant where the background flow was compressive rather than extensive. For this time-dependent case they also identified successive transitions to higher-order buckling modes (see Fig. 2 of [41]) as a forcing parameter, equivalent to η, was increased. The first transition to

buckling takes place at the same effective value of η (153.2) as for the pure strain case. Using the local SBT formulation, their numerical simulations studied the very nonlinear shape dynamics of the fiber above the buckling transition (see Fig. 1.3c). They also showed that fiber buckling past the first transition gave rise to positive first normal stress differences, and that the predicted threshold to buckling agreed well with the onset of positive first normal stress differences in shearing experiments of nylon fibers in glycerin [42]. Their simulations also predicted that large amplitude flexing of the fiber at large values of η could give rise to negative normal stress differences.

The stability of free fibers in linear flows - Experimental observations

The buckling of flexible fibers in viscous flows has been investigated experimentally in two different flow situations: fibers at or near hyperbolic stagnation points or fibers moving in shear flows (simple shear or Poiseuille flow).

The onset of fiber buckling with approach to a stagnation point has been investigated in a macroscopic system by Wandersman *et al.* [25] who used centimetric fibers made of a soft elastomer. These fibers moved across a viscous cellular flow consisting of a planar array of magnetically driven, counter-rotating vortices. Each 2×2 set of vortices then surrounds a hyperbolic stagnation point. Above a critical value of the control parameter η, fibers are observed to buckle (Fig. 1.2a). With increasing η more complex fiber shapes are observed (Fig. 1.2b), corresponding to the eigen-shapes predicted by the linear stability analysis discussed in Sect. 1.2. The fluid forcing regimes in which these different modes are observed was found to be in rough agreement with theoretical predictions. The interesting transport dynamics of these fibers across the cellular array will be discussed in Sect. 1.4.3.

Kantsler and Goldstein [36] have investigated the deformation of a micrometric actin fiber held at a stagnation point created in a micro-fluidic cross-slot device (Fig. 1.2c) where, unlike the experiments of Wandersman *et al.* [25], transport dynamics do not play a role. This study reported the deformation of the actin fiber as a function of the control parameter $|\Sigma| = \eta/4\pi^4$, and is shown in Fig. 1.2d. This work was also in good agreement with the linear stability analysis for fibers in a simple 2D straining flow. Unlike the larger scale fibers used in the study of Wandersman *et al.* [25], microscopic actin fibers are subject to Brownian fluctuations, though their contribution to the dynamics did not appear to have an substantial influence on the buckling thresholds.

The deformation of elastic fibers under simple shear was studied by Forgacs and Mason [44]. They performed experiments using millimetric elastomer fibers in corn syrup, driven between two counter-rotating cylinders in a Couette geometry. They identified a critical fiber length above which fiber buckling occurs, in qualitative agreement with their theoretical analysis. Visual observation showed very complex dynamics (Fig. 1.3a) such as "snake turns", very similar to the numerical results of Becker and Shelley [41] (Fig. 1.3c), Stockie and Green [11], Delmotte *et al.* [18] and Nguyen and Fauci [13] (Fig. 1.3d). Well above the onset of buckling, more complex dynamics such as helix formation, rotation, and coiling were also reported. Harasim *et al.* [35] studied the motion and deformations of actin fibers in a micro-fluidic Poiseuille flow (Fig. 1.3b). In their study the fiber lengths were on the order of 10 μm, which is not well separated from the channel widths, and so one expects continuous bending by the Poiseuille flow rather than a buckling transition. The relation between fiber deformation and the period of the

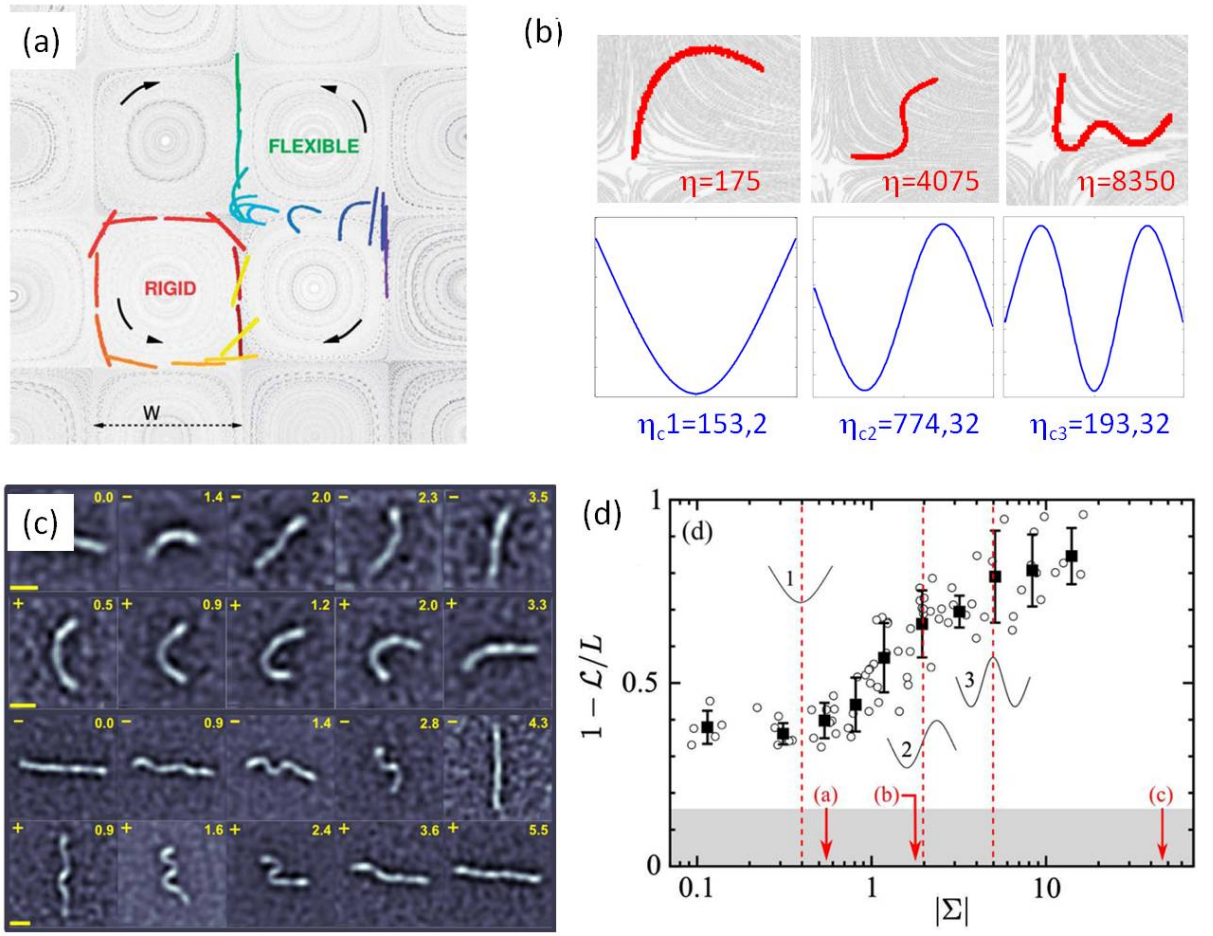

Figure 1.2: Fibers at or close to a stagnation point **(a)** A centimetric fiber ($W = 3$ cm), made from a silicon elastomer, is transported in a viscous cellular flow created by electromagnetic forcing. The more rigid fiber, bottom left, does not deform whereas the more flexible fiber, top right, undergoes a buckling instability. From Wandersman *et al.* [25]. **(b)** Dxperimental fiber shapes at different control parameters (top row) and shapes from linear stability analysis (see Sect. 1.2) together with the critical values of the control parameter η_c. From Quennouz [43]. **(c)** Actin fibers at a stagnation point in a micro-fluidic device. Snapshots are shown as a function of time for increasing values of the control parameter (from top to bottom). The scale bar corresponds to 3 μm. From Kantsler and Goldstein [36], as is: **(d)** Fiber compression as a function of the control parameter $|\Sigma| = \eta/4\pi^4$.

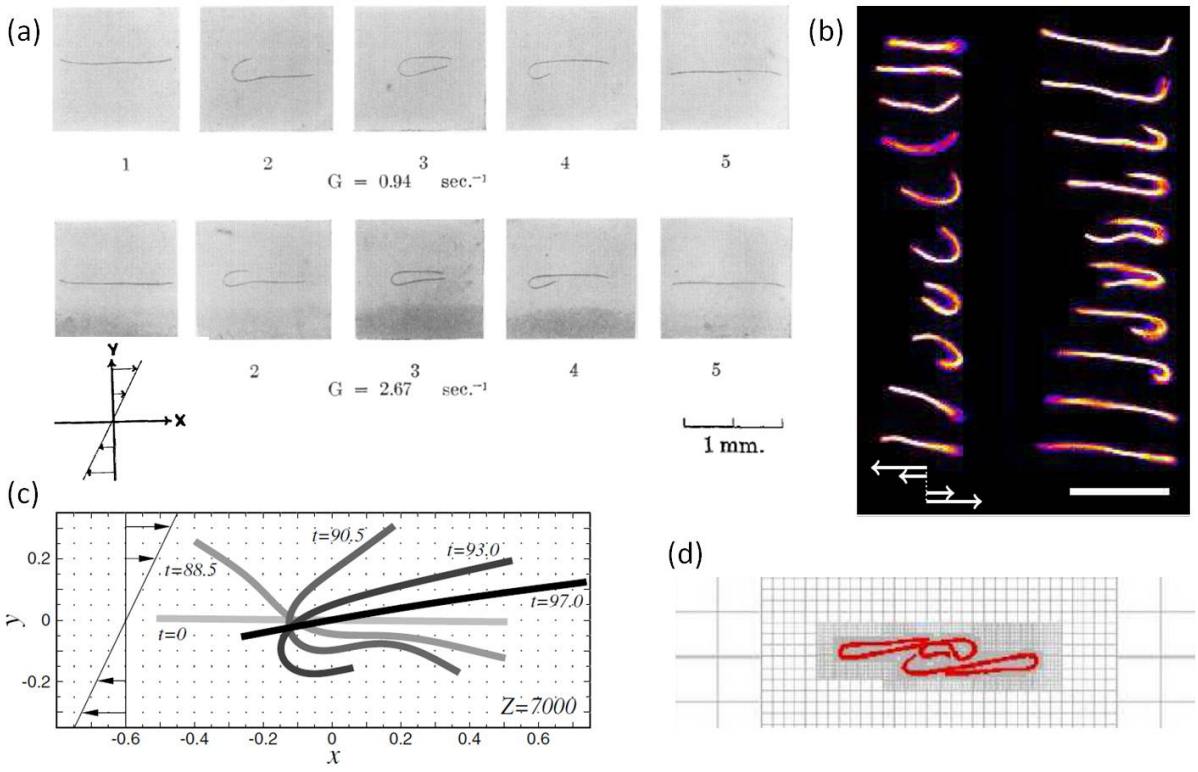

Figure 1.3: Fibers in shear flows **(a)** Elastomeric fibers in corn syrup in a simple shear flow created between two counter-rotating cylinders. From the top row to the bottom row the shear rate is increased. So called snake turns are observed. From Forgacs and Mason [24]. **(b)** Actin fibers in a Poiseuille flow in a micro-fluidic geometry. The fiber length is changed from left to right. The scale bar corresponds to 10 μm. From Harasim *et al.* [35]. **(c)** From simulations using local SBT, the buckling of a flexible fiber in a shear flow at $\eta = 7000$. From Becker and Shelley [41]. **(d)** Using an adaptive version of the immersed boundary method, simulation shows very complex fiber shapes emerging in a shear flow. From Nguyen and Fauci [13].

Jeffrey orbits [39] has also been discussed and the studies of Forgacs and Mason [24], Harasim *et al.* [35], Slowicka *et al.* [45] all attempted to map the observed orbits onto the prediction for Jeffrey orbits of elongated ellipsoids [39].

The buckling of anchored fibers in impinging flows – Mathematical analysis

Using local SBT, Guglielmini *et al* [46] have investigated the stability of elastic fibers when held against impinging linear or quadratic stagnation point flows; see Fig. 1.4.

For the linear background flow, $\mathbf{U} = (x, -y)$, or the quadratic flow, $\mathbf{U} = (xy, -y^2)$, the straight filament, $\mathbf{X}(s) = (0, s)$ $(0 \leq s \leq 1)$, whose end point at $s = 0$ is held fixed at $\mathbf{x} = \mathbf{0}$, provides an exact solution to Eqs. (1.5) & (1.6). The associated base tension is quadratic in s for the linear flow, and cubic in s for the quadratic flow. In either case the base tension is negative, and hence compressive. At $s = 1$, "free" boundary conditions are assumed, while at the fixed end $s = 0$ they consider the clamped boundary condition, i.e. $f_s = 0$ within the linearized

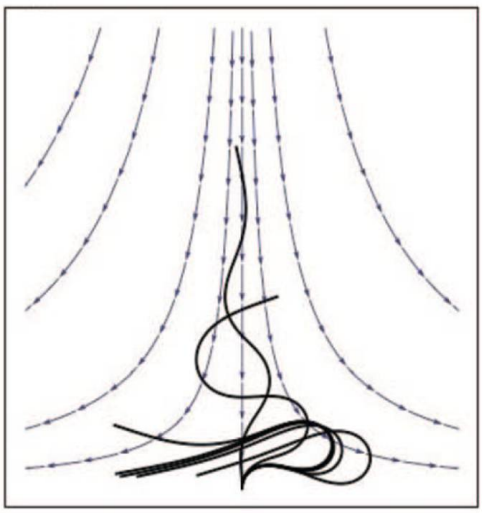

Figure 1.4: Simulations of the buckling instability of a clamped fiber in a linear background flow. From Guglielmini *et al.* [46].

dynamics for a filament held straight at the base, and the hinged boundary condition, $f_{ss} = 0$ (free to rotate with zero applied torque). To identify critical values in η for buckling transitions they discretized the linearized dynamics equations (i.e., Eq. (1.12) for the linear flow case) and its boundary conditions using Chebychev polynomials in s and posed it as a generalized finite-dimensional eigenvalue problem for growth rates.

For the clamped filament a first unstable mode corresponding to bending is identified for both flow fields. The second unstable mode corresponds to a buckling instability (Fig. 1.4) and the threshold is found to be slightly lower compared to the first buckling mode of a free fiber. The hinged fiber is always unstable to rotation around the base. Higher modes correspond to buckling instabilities, and in this case the threshold for buckling is significantly smaller compared to free fibers.

To our knowledge no systematic study of the bucking of anchored fibers in impinging flows has as yet been undertaken. However, experiments performed on very long fibers flowing in rough fractures have revealed strong deformation of these fibers when temporarily pinned at local asperities [47].

The buckling of sedimenting fibers – Mathematical analysis

Li *et al.* [48] studied the sedimentation of flexible filaments under gravity in a viscous fluid. They characterized the competition between elastic and viscous forces, induced by gravity, by an elasto-gravitation number $\beta = \pi Y a^4/(4F_g L^2)$. Using a formulation and methods very similar to those of Tornberg and Shelley [7], they argue that for a fiber settling parallel to gravity, buckling will occur in an interesting fashion. For a straight, slender filament of ellipsoidal shape, they show that their nondimensional fiber tension is given by a cubic polynomial in s; *cf.* Eq. (1.10):

$$\bar{T} = 2s(s^2 - 1/4) \tag{1.13}$$

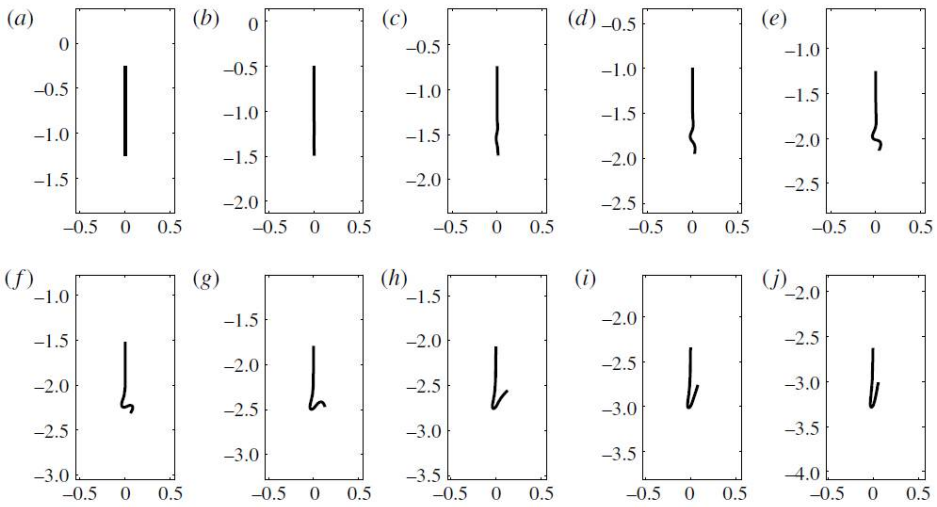

Figure 1.5: Simulations of the buckling instability of a very flexible fiber sedimenting downwards in a viscous flow. From Li *et al.* [48].

where $-1/2 \leq s \leq 1/2$ and $s = 1/2$ labels the leading end of the fiber as it settles downwards. In this situation the tension is compressive in the leading half, and extensive in the trailing half. This division arises because the greater fiber mass per unit length near the fiber midpoint "pushes down" on the leading half, and "pulls down" upon the trailing half. Local flows generated by the fiber's descent reinforce this effect. The authors identified a critical value, β_c, above which the straight fiber is unstable to buckling of its leading half. Fully nonlinear simulations of the results of that instability are shown in Fig. 1.5. The shapes of sedimenting isolated filaments [18] or pairs of interacting filaments [49] have also been investigated using bead models.

To our knowledge no experimental investigation of these predictions has yet been undertaken.

1.4.2 Deformation of fibers

In subsection 1.4.1 we discussed the buckling of anchored fibers under a compressive flow. Such anchored fibers are also deformed by viscous flows when the flow direction is not parallel to the fiber orientation. In this case no threshold for deformation exists, for a number of simple flow geometries this situation is akin to a bending beam where viscous forces play the role of a gravitational load. For more complex flows, as for example in confined geometries or flows with curved streamlines, numerical approaches have been used to determine the fiber deformation.

Passive anchored fibers, such as the primary cilium, are found in biological systems, and can also form spontaneously under flow conditions as is seen in the formation of biofilm streamers. In engineered micro-fluidic flow geometries, micro-fabricated anchored fibers can be used as flow sensors, or conversely the micro-fluidic flows can be used to measure the bending properties of unknown materials. Fixed, driven fibers have also been studied to understand the locomotion of micro-organisms at low Reynolds number.

Rusconi *et al.* [50, 51] have shown that biofilms formed by bacterial communities develop

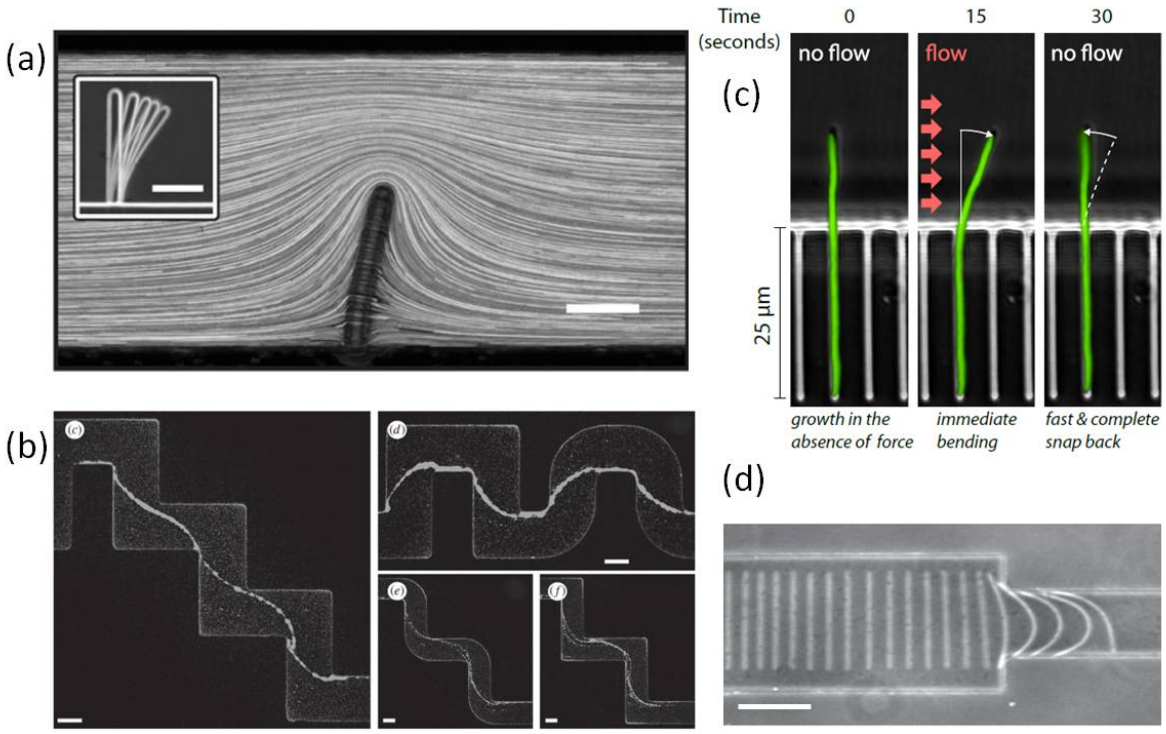

Figure 1.6: Fiber bending. **(a)** A polymeric fiber, fabricated by an *in-situ* UV projection method, anchored at a channel wall perpendicular to the flow direction. Streamlines visualized using passive tracer particles. Inset is deformation of the same fiber with increasing flow rate. Scale bars are 100 μm. From Wexler *et al.* [33]. **(b)** Biofilm streamers formed with wild-type *Pseudomonas aeruginosa* bacteria in micro-fluidic channels of different geometries. The streamers are visualized at mid-height of the micro-fluidic channel in an unconfined situation (streamer diameter much smaller than channel height). The scale bar represents 100 μm. From Rusconi *et al.* [50, 51]. **(c)** A flexible fiber formed by growing cells of *E. coli* bacteria, anchored in a micro-channel perpendicular to the flow direction. Adapted from Amir *et al.* [52] **(d)** Polymeric fibers (as in **(a)**) approaching a restriction in a micro-channel. Deformation occurs when the fibers get stuck at the restriction. From Berthet [29].

as long filamentous elastic structures, called streamers, under flow. Their formation can be triggered by the laminar flow of a fluid around re-entrant corners (Fig. 1.6b) and their presence can lead to catastrophic disruption of flows in environmental and medical systems due to clogging [53]. The shape of these streamers under flow is a function of the ratio of the viscous to elastic forces encapsulated in η. The shape of elastic fibers within flows with curved streamlines has been determined numerically by Autrusson *et al.* [54] for fibers anchored, either hinged or clamped, at given positions near a two-dimensional corner. This work shows that, due to tension and bending forces within the fibers, the fibers do not align with the flow but rather cross flow streamlines. This is in agreement with the experimental observations from Rusconi *et al.* [50, 51] shown on Fig. 1.6b.

Amir *et al.* [52] studied the flow-induced bending of single-cell *Escherichia coli* growing from slits in the side-walls of a micro-fluidic channel. (Fig. 1.6c). Their goal was to investigate growth of the organism's cell wall. By applying a flow perpendicularly to the cells, the experimental set-up corresponds to a simple bending beam experiment where the force applied to the cell results from the viscous friction of the fluid. By estimating this viscous force and using linear elasticity theory, the authors were able to estimate the bending stiffness of the *E. coli* cells from the measured deflection. The simple hydrodynamic set-up gave values similar to those obtained using much more costly techniques such as AFM measurements.

Another biological example of a flexible fiber attached to a wall and subject to flow forcing is the *primary cilium*. The primary cilium is a non-motile isolated hair-like protrusion from a cell into the extracellular space and is found in a wide variety of vertebrate cells. Among other things, the primary cilium is believed to act as a mechanoreceptor by bending in response to flow as is observed in kidney tubule cells. Its dynamics has been investigated in a combined experimental and theoretical study by Young *et al.* [55]. The authors showed that the bending dynamics of the primary cilium could be accurately described as an elastic beam whose base, or anchor point, is attached to a rotational nonlinear spring. This spring models the mechanical response of the basal cell membrane as it is distorted by the bending of the cilium.

Fibers fabricated by the *in-situ* UV projection method (see section 1.3) have been observed to bend in micro-fluidic flow geometries. In a confined flow geometry where the diameter of the fibers approaches the channel height, freely moving fibers approaching a restriction were found to bend before flowing through (Fig. 1.6d). The bending occurs in a situation where both ends of the fiber are pushed against the entry of the restriction, and corresponds again to a simple beam bending experiment. The force exerted on the fiber can, in the situation where the fiber blocks the whole channel width, be easily estimated using lubrication theory, and so again the mechanical properties of the fiber can be estimated [34].

The flow geometry becomes more complex when the fiber is attached to only one side wall in a confined channel. Then liquid can flow above or around the fiber which only partially blocks the channel. An experimental realization by Wexler *et al.* [33] uses fibers, attached to the wall of a micro-channel and perpendicular to the flow direction. The streamlines are visualized using tracer particles and show the complex flow profile (Fig. 1.6a). A theoretical model [33] gave insight into the competition between bending and leakage flow, showing favorable agreement with the experimental results, and was also used to measure fiber rigidity (as was done for *E. coli* cells). By knowing its mechanical properties, such a fiber could, in the future, be used as a flow sensor in micro-fluidic devices.

Driven elastic fibers moving in a viscous fluid become deformed as has been observed by

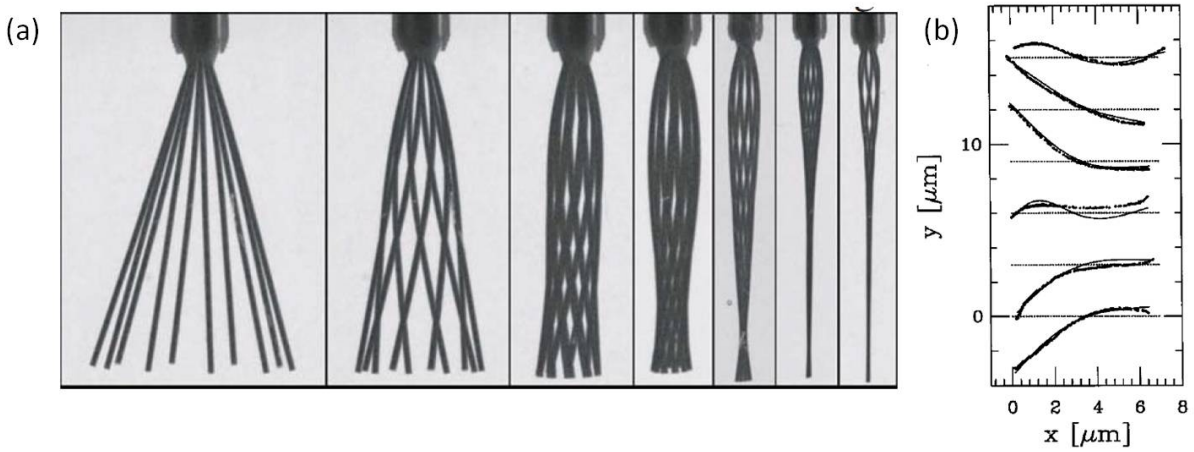

Figure 1.7: Driven fibers. **(a)** A centimetric fiber being rotated in a viscous fluid. From left to right the control parameter η is increased by increasing the fiber length. Superpositions of snapshots at different times are shown over one rotation period. From Coq *et al.* [56]. **(b)** Successive shapes of an actin filament attached to a magnetic bead beating in a viscous fluid as a function of time (snapshots shown every 80ms) and analytical solution of the time dependent shapes. From Wiggins *et al.* [57].

Qian *et al.* [58] and Coq *et al.* [56]. Both studied the driven rotation of long elastic fibers tilted relative to their rotation axes in a viscous fluid and observed a transition from a straight fiber towards a helical shape (Fig. 1.7a). The induced helicity generates a propulsive force along the axis of rotation. A later study investigated the collective dynamics of a micro-carpet made of hundreds of slender magnetic rods [59]. In early work Wiggins *et al.* [57] studied the deformation of an elastic fiber attached to a bead that was driven by an optical trap (Fig. 1.7b). Also in this case the deformation led to a propulsive force. Such experiments have helped to understand the mechanisms of microorganismal propulsion, the action of ciliar carpets as are found in the human lung, and symmetry breaking in early development [60, 61].

1.4.3 Deformation and Transport

That fibers can be deformed by flow is expected to modify their transport properties. This link has been established theoretically in a number of situations, and has been studied, as yet somewhat less, through experiments.

From their numerical study of fiber-flow interactions Young and Shelley [40] predicted that flexible fibers could move as random walkers across a closed stream-line flow. Here the background flow is a two-dimensional array of counter-rotating vortices where every 2×2 subarray of vortices is centered on a hyperbolic fixed point for the flow; see Fig. 1.8b. Roughly speaking, if a fiber is floppy enough it will tend to be trapped, once there, inside of vortices. However, if it is between vortices it is drawn towards the stagnation point while being stretched out by the local hyperbolic flow. Nearing the fixed point is becomes compressed by viscous stresses in the manner described by their linear analysis, and the fiber frequently buckles. This buckling, with its many degrees of freedom, yields an effective randomness in the direction from which the

fiber exits the stagnation point zone. This dynamics also tends to keep fibers along the backbone of the flow composed of stagnation points and their connecting stagnation streamlines. The precise transport properties also depend in a non-trivial way on fiber flexibility and length. Numerical simulations by Manikantan and Saintillan [62] confirmed these basic findings and addressed the role of Brownian fluctuations which were shown to increase trapping of filaments in vortices and thus also decrease transport across the vortex array. See Bouzarth *et al.* [22] and Young [63] for a numerical study of two fibers interacting in such cellular flows.

While the experimental realization of such a flow is difficult, Wandersman *et al.* [25] have shown that a flexible fiber can indeed escape more quickly from a given vortex of a cellular flow compared to a rigid fiber. The complex fiber dynamics of such an escape is shown on Fig. 1.8c. Note that rigid fibers also show non-trivial dynamics in such flows when the fiber length becomes comparable to the cell size of the cellular flow.

In Poiseuille channel flow, flexible fibers have been shown to exhibit stable trajectories and to accumulate at distances from the wall that are a function of their flexibility [45]. Reddig and Stark [64] and Chelakkot *et al.* [65] have shown numerically that semi-flexible polymers, described using bead models, show strong cross-stream migration. Using semiflexible actin filaments in micro-fluidic geometries Steinhauser *et al.* [37] have shown experimentally that shear induced migration takes place towards the walls in very confined channels.

The theoretical work of Li *et al.* [48] shows that the sedimentation dynamics of fibers is substantially altered by their flexibility. If the filament is allowed to bend even slightly in response to gravitational load, there can arise a coupling between its translational and rotational motions, leading to its reorientation with respect to gravity. Because the orientation of the filament directly determines the direction of its velocity this leads to a non-trivial translational motion in both vertical and horizontal directions. In particular, the trajectories of flexible sedimenting fibers are restricted to a cloud whose envelope is determined by the elasto-gravitation number β introduced in section 1.4.1.

And finally, buckling instabilities can perform important functions for living micro-organisms. As shown by Son *et al.* [66], some mono-flagellated bacteria perform a random re-orientation of their swimming direction (a form of run-and-tumble dynamics) by inducing a buckling in the flagellar "hook" at the base of the flagellum; see Fig. 1.8a. This is accomplished by reversing the flagellar motor direction which produces a compressive load on the flagellar hook.

1.4.4 Fiber-fiber interactions and suspension dynamics

The majority of the work reviewed thus far concerns the interactions of single elastic fibers with background flows. There have been comparatively few theoretical or numerical studies on how multiple fibers, or ensembles of fibers, interact with each other. Recent work in this area is reviewed nicely by Hämäläinen *et al.* [15] but we shall mention a few here. Several studies (e.g. [17, 67, 68]) studied the rheology of flexible fiber suspensions by treating each fiber as a chain of linked rigid bodies (e.g. spheres, spheroids, rods) that experience local drag and interact with each other through short-range forces (e.g. repulsion, lubrication, friction), while neglecting long-ranged hydrodynamic interactions or only including a subset of them. Their inclusion is of course very costly in terms of simulation time.

Joung *et al.* [69] developed a bead-and-rod model of a slightly flexible fiber that accounted for short range lubrication interaction between interacting fibers, as well as long-ranged hy-

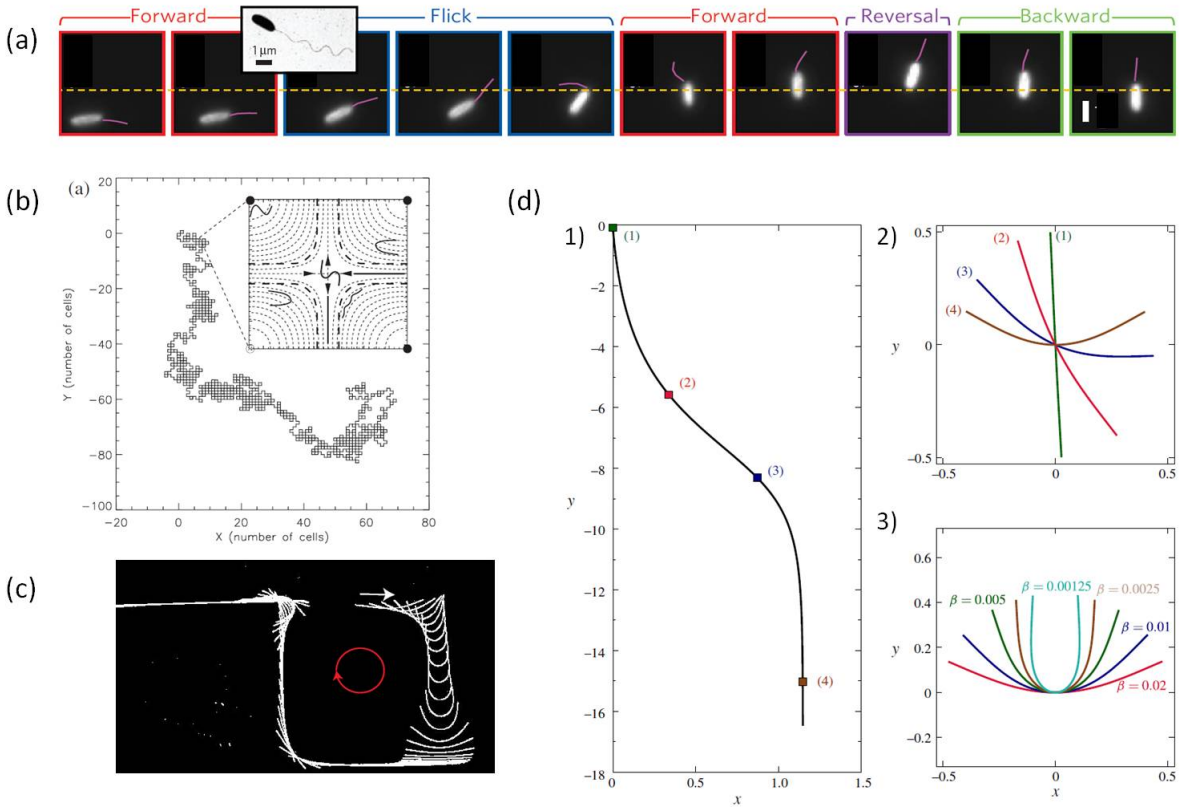

Figure 1.8: **(a)** High-speed images of a mono-flagellated *Vibrio alginolyticus* bacterium show the microorganism executing an abrupt and random change in swimming direction. This is mediated by a buckling instability of the hook linking the flagellum to the body. Images are shown every 10 ms and the scale bar corresponds to 3 μm. Adapted from Son *et al.* [66]. **(b)** Simulations of the random walk of a flexible filament across a cellular flow. From Young and Shelley [40]). **(c)** Dynamics of a flexible macroscopic filament escaping from a vortex within a cellular flow. From experiments of Quennouz [43]). **(d)** From simulations, (1) the trajectory of a sedimenting fiber and (2) corresponding filament shapes. (3) Steady state shapes of fibers with increasing flexibility (decreasing β). From Li *et al.* [48].

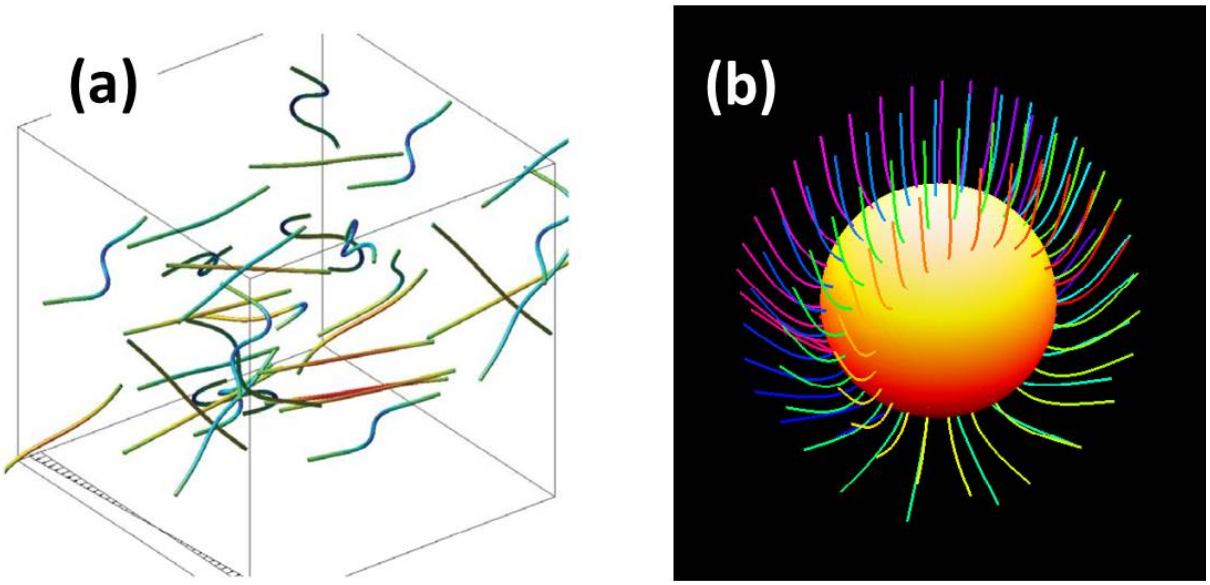

Figure 1.9: Simulations of flows with many flexible fibers. **(a)** The buckling dynamics of 25 flexible fibers interacting in an oscillating shear flow. The numerical method is based upon nonlocal SBT. Adapted from Tornberg and Shelley [7]. **(b)** From a simulation that combines nonlocal SBT with boundary integral methods for immersed surfaces, the bending dynamics of 100 flexible fibers attached to a sedimenting sphere. From Nazockdast and Shelley (in preparation).

drodynamic interactions between beads. In a periodic cell they simulate up to 90 fibers, and recover, for example, the experimental result of Goto [42] that flexibility increases the suspension viscosity relative to the case of rigid rods. Tornberg and Shelley [7] use nonlocal SBT and a continuum description of the fiber and its forces to simulate 25 filaments in a periodic box and interacting under periodic shear. One interesting aspect of this simulation was the demonstration that hydrodynamic interactions were sufficient to drive buckling instabilities of the initially straight fibers in the suspension (Fig. 1.9a). In recent modeling work related to subcellular processes in developmental biology, Nazockdast and Shelley have been merging nonlocal SBT with boundary integral methods for immersed surfaces. Using such an approach, Fig. 1.9b shows the hydrodynamically mediated bending of 100 flexible fibers, or hairs, attached to a solid sphere held fixed against an upward flow (in preparation). In building tools for simulating papermaking, Lindstrom and Uesaka (see, for example, [16]) have developed an approach that is a hybrid of that developed by [17] where the the fiber is treated as a linked chain of ellipsoids, and the immersed boundary type method [10] where fiber forces drive the immersing fluid motions through a coupling term in the large-scale momentum equations.

1.5 Summary and Outlook

In this short review we have surveyed the interaction of flexible fibers with low Reynolds number flows, focusing mostly on the central role played by buckling instabilities but also on the roles of bending and confinement. While we have achieved a good theoretical understanding of how single, or a few, fibers interact with a flow, much less is known of the ensemble behavior of suspensions of flexible fibers. This is due in large part to the computational cost of simulating such suspensions though there have been recent and dramatic advances in simulating related problems using fast summation strategies implemented within massively parallel environments [70]. Another obstacle to progress is the lack of good mathematical tools for modeling suspensions at the continuum level when the microstructure has many degrees of freedom.

From the experimental point of view, successively more precise model systems – both micro-fabricated and biological – have been developed over the last years, leading to a number of careful investigations of single fiber dynamics under flow. These observations have led to a more precise understanding of biological systems and have paved the way to applications in the engineering of micro-fluidic devices. While accessing macroscopic suspension properties, in particular for semi-dilute or concentrated suspensions, does not require particular experimental care, the link between macroscopic behaviors and fiber flexibility is not yet well established.

One reason for desiring such an understanding is that fiber suspensions may show new dynamical states, perhaps akin to the viscoelastic turbulence evinced by driven polymer suspensions, and perhaps intimately related to the stretch-coil instability analog to the coil-stretch of coiled polymers. Concentration effects are also especially interesting in flexible fiber suspension, as one anticipates not only overlap concentration effects, but also new mechanics arising from ordering transitions as are seen in polymer liquid crystal systems. Finally, a deeper understanding of fiber suspensions may shed light onto the dynamics of biological structures, such as the centrosomal microtubule array and the mitotic spindle, which are both self-assembled structures that mediate cell division.

Acknowledgements: We thank Olivia du Roure, David Saintillan and Harishankar Manikan-

tan for a careful reading of our manuscript. MJS acknowledges the support of the US Department of Energy, National Science Foundation, and the National Institutes of Health. AL acknowledges support from the European Commission under FP7, and from Schlumberger Ltd.

Bibliography

[1] J. Keller and S. Rubinow, *J. Fluid Mech.*, 1976, **75**, 705–714.

[2] C. Pozrikidis, *Boundary Integral and Singularity Methods for Linearized Viscous Flow*, Cambridge University Press, 1992.

[3] R. Johnson, *J. Fluid Mech.*, 1980, **99**, 411–431.

[4] T. Götz, *PhD thesis*, University of Kaiserslautern, Germany, 2000.

[5] M. Shelley and T. Ueda, Advances in Multi-Fluids Flows, 1996, pp. 415–425.

[6] M. Shelley and T. Ueda, *Phys. D*, 2000, **146**, 221–245.

[7] A.-K. Tornberg and M. Shelley, *J. Comp. Phys.*, 2004, **196**, 8–40.

[8] A. Tornberg and K. Gustavsson, *J. Comp. Phys.*, 2006, **215**, 172–196.

[9] D. Saintillan, E. Darve and E. S. G. Shaqfeh, *Phys. Fluids*, 2005, **17**, 033301.

[10] C. Peskin, *Acta Num.*, 2002, **11**, 479–517.

[11] J. M. Stockie and S. I. Green, *J. Comp. Phys.*, 1998, **147**, 147–165.

[12] S. Lim and C. Peskin, *SIAM J. Sci. Comput.*, 2004, **25**, 2066–2083.

[13] H. Nguyen and L. Fauci, *Submitted*, 2014.

[14] B. Griffith, R. Hornung, D. McQueen and C. Peskin, *J. Comp. Phys.*, 2007, **223**, 10–19.

[15] J. Hämäläinen, S. Lindström, T. Hämäläinen and H. Niskanen, *J. Eng. Math.*, 2011, **71**, 55–79.

[16] S. Lindström and T. Uesaka, *Phys. Fluids*, 2009, **21**, 083301.

[17] L. Switzer and D. Klingenberg, *Int. J. of Multi. Flow*, 2004, **30**, 67–87.

[18] B. Delmotte, E. Climent and F. Plouraboué, *submitted*, 2014.

[19] R. Cortez, *SIAM J. Sci. Comp.*, 2001, **23**, 1204–1225.

[20] H. Flores, E. Lobaton, S. Méndez-Diez, S. Tlupova and R. Cortez, *Bull. Math. Bio.*, 2005, **67**, 137–168.

[21] D. J. Smith, *Proceedings of the Royal Society A: Mathematical, Physical and Engineering Science*, 2009, **465**, 3605–3626.

[22] E. Bouzarth, A. Layton and Y.-N. Young, *Int. J. Num. Meth. Biomed. Eng.*, 2011, **27**, 2021–2034.

[23] S. D. Olson, S. Lim and R. Cortez, *J. Comp. Phys*, 2013, **238**, 169–187.

[24] O. L. Forgacs and S. G. Mason, *J. Coll. Sci.*, 1959, **14**, 473–491.

[25] E. Wandersman, N. Quennouz, M. Fermigier, A. Lindner and O. du Roure, *Soft Matter*, 2010, **6**, 5715–5719.

[26] G. M. Whitesides, *Nature*, 2006, **442**, 368–73.

[27] J. K. Nunes, H. Constantin and H. a. Stone, *Soft Matter*, 2013, 4227–4235.

[28] H. Berthet, M. Fermigier and A. Lindner, *Phys. Fluids*, 2013, **25**, 103601.

[29] H. Berthet, *PhD thesis*, UPMC, Paris, France, 2012.

[30] D. Dendukuri, D. C. Pregibon, J. Collins, T. A. Hatton and P. S. Doyle, *Nat. Mat.*, 2006, **5**, 365–9.

[31] D. Dendukuri, S. S. Gu, D. C. Pregibon, T. A. Hatton and P. S. Doyle, *Lab on a chip*, 2007, **7**, 818–28.

[32] C. Goubault, F. Leal-Calderon, J.-L. Viovy and J. Bibette, *Langmuir*, 2005, **21**, 3725–9.

[33] J. S. Wexler, P. H. Trinh, H. Berthet, N. Quennouz, O. du Roure, H. E. Huppert, A. Linder and H. A. Stone, *J. Fluid Mech.*, 2013, **720**, 517–544.

[34] C. Duprat, H. Berthet, J. Wexler, O. du Roure and A. Lindner, *in preparation*, 2014.

[35] M. Harasim, B. Wunderlich, O. Peleg, M. Kröger and A. R. Bausch, *Phys. Rev. Lett.*, 2013, **110**, 108302.

[36] V. Kantsler and R. E. Goldstein, *Physical review letters*, 2012, **108**, 038103.

[37] D. Steinhauser, S. Koster and T. Pfohl, *ACS Macro Letters*, 2012, **1**, 541–545.

[38] T. Sanchez, D. Chen, S. DeCamp, M. Heymann and Z. Dogic, *Nature*, 2012, **491**, 431–434.

[39] G. Jeffrey, *Proc. Roy. Soc. A*, 1922, 102–161.

[40] Y.-N. Young and M. Shelley, *Phys. Rev. Lett.*, 2007, **99**, 058303.

[41] L. Becker and M. Shelley, *Phys. Rev. Lett.*, 2001, **87**, 198301.

[42] S. Goto, H. Nagazono and H. Kato, *Rheo. Acta*, 1986, **25**, 246–256.

[43] N. Quennouz, *PhD thesis*, UPMC, Paris, France, 2013.

[44] O. L. Forgacs and S. G. Mason, *J. Coll. Sci.*, 1959, **14**, 457–472.

[45] A. M. Slowicka, E. Wajnryb and M. L. Ekiel-Jezewska, *Euro. Phys. J. E*, 2013, **36**, 9844.

[46] L. Guglielmini, A. Kushwaha, E. S. Shaqfeh and H. A. Stone, *Physics of Fluids*, 2012, **24**, 123601.

[47] M. V. D'Angelo, B. Semin, G. Picard, M. E. Poitzsch, J. P. Hulin and H. Auradou, *Trans. Porous Med.*, 2009, **84**, 389–408.

[48] L. Li, H. Manikantan, D. Saintillan and S. Spagnolie, *J. Fluid Mech*, 2013, **735**, 705–736.

[49] I. Llopis, I. Pagonabarraga, M. Cosentino Lagomarsino and C. Lowe, *Phys. Rev. E*, 2007, **76**, 061901.

[50] R. Rusconi, S. Lecuyer, L. Guglielmini and H. a. Stone, *J. Roy. Soc. Interface*, 2010, **7**, 1293–9.

[51] R. Rusconi, S. Lecuyer, N. Autrusson, L. Guglielmini and H. a. Stone, *Biophys. J.*, 2011, **100**, 1392–9.

[52] A. Amir, F. Babaeipour, D. R. Nelson and S. Jun, 2013, 1–40.

[53] K. Drescher, Y. Shen, B. L. Bassler and H. a. Stone, *Proc. Nat. Acad. Sci. USA*, 2013, **110**, 4345–50.

[54] N. Autrusson, L. Guglielmini, S. Lecuyer, R. Rusconi and H. A. Stone, *Physics of Fluids*, 2011, **23**, 063602.

[55] Y.-N. Young, M. Downs and C. R. Jacobs, *Biophys. J.*, 2012, **103**, 629–39.

[56] N. Coq, O. du Roure, J. Marthelot, D. Bartolo and M. Fermigier, *Phys. Fluids*, 2008, **20**, 051703.

[57] C. H. Wiggins, D. Riveline, a. Ott and R. E. Goldstein, *Biophys. J.*, 1998, **74**, 1043–60.

[58] B. Qian, T. Powers and K. Breuer, *Phys. Rev. Lett.*, 2008, **100**, 078101.

[59] N. Coq, A. Bricard, F.-D. Delapierre, L. Malaquin, O. du Roure, M. Fermigier and D. Bartolo, *Phys. Rev. Lett.*, 2011, **107**, 014501.

[60] N. Hirokawa, Y. Tanaka, Y. Okada, and S. Takeda, *Cell*, 2006, **125**, 3345.

[61] J. Gray, *Cell Movements: From Molecules to Motility*, Garland, New Yor, 2001.

[62] H. Manikantan and D. Saintillan, *Phys. Fluids*, 2013, **25**, 073603.

[63] Y.-N. Young, *Phys. Rev. E*, 2009, **79**, 046317.

[64] S. Reddig and H. Stark, *J. Chem. Phys.*, 2011, **135**, 165101.

[65] R. Chelakkot, R. G. Winkler and G. Gompper, *EPL*, 2010, **91**, 14001.

[66] K. Son, J. S. Guasto and R. Stocker, *Nat. Phys.*, 2013, **9**, 494–498.

[67] S. Yamamoto and T. Matsuoka, *J. Chem. Phys.*, 1995, **102**, 2254–2260.

[68] R. Ross and D. Klingenberg, *J. Chem. Phys.*, 1997, **106**, 2949–2960.

[69] C. Joung, N. Phan-Thien and X. Fan, *J. Non-Newt. Fluid Mech.*, 2001, **99**, 1–36.

[70] A. Rahimian *et al.*, Proceedings of the 2010 ACM/IEEE International Conference for High Performance Computing, Networking, Storage and Analysis, 2010, pp. 1–11.